

Electronic Supplementary Information

In situ phosphorization strategy towards doped Co₂P scaffolded within echinus-like carbon for overall water splitting

Hui Li,[‡] Si-Min Xu,[‡] Yaru Li, Hong Yan* and Sailong Xu*

State Key Laboratory of Chemical Resource Engineering, Beijing University of Chemical Technology, Beijing 100029, China

[‡]H.L. and S.-M.X. contributed equally to this work.

*Corresponding authors. E-mails: xusl@mail.buct.edu.cn (S.X.); yanhong@mail.buct.edu.cn (H.Y.)

Experimental Section

1. Preparation of Materials

SDP/MCo-LDH precursor The SDP/CoFe-LDH precursor was synthesized by using a conventional precipitation method. In brief, a mixture of Co(NO₃)₂·6H₂O (8 mmol), Fe(NO₃)₃·9H₂O (2 mmol), urea (20 mmol), and SDP (14 mmol) was dissolved in 150 mL of deionized and decarbonated water, followed by strongly stirring under N₂ atmosphere for 30 min to form a purple solution at 70 °C. The slurry was then transferred into a Teflon-lined stainless steel autoclave and kept at 150 °C for 15 h. The SDP/CoFe-LDH precursor was obtained by washing with distilled water and ethanol several times, and drying at 60 °C for 24 h in a vacuum oven.

Similarly, the precursors of SDP/NiCo-LDH and SDP/Co(OH)₂ were prepared under the same experimental conditions, except for using nickel salt to replace ferric salt and no other salt, respectively.

Preparation of MCo₂P@C products All the as-prepared precursors were heated to 800 °C at a ramping rate of 1 °C min⁻¹ for 6 h under Ar flow in a tube furnace to obtain echinus-like carbon-coated (MCo)₂P/C nanocomposites.

2. Characterization

X-ray diffraction (XRD) pattern was recorded with a diffract-meter (Shimadzu XRD-6000) with a filtered Cu Kα radiation (λ = 1.5418 Å). The SEM observation was performed

on a ZEISS Supra 55 equipped with energy-dispersive X-ray spectroscopy. Transmission electron microscopy (TEM) and high-resolution TEM (HRTEM) images were carried out on a JEOL electron microscope (JEM-2100) with an accelerating voltage of 200 kV. X-ray photoelectron spectroscopy (XPS) were recorded on a Thermo VG Scientific spectrometer. Raman spectrometer (Renishaw RM2000) was utilized to collect Raman spectroscopy, which is equipped with a 532 nm excitation laser (laser spot size of 0.5 μm) and operated at a low power level (ca. 2 mW). Elemental analysis for metal ions was employed using a Shimadzu inductively coupled plasma optical emission spectrometer (ICP-OES). Cs-corrected Scanning Transmission Electron Microscopy (STEM) imaging and Electron energy-loss spectra (EELS) diagram was recorded using JEOL JEM-ARM200F (200 kV) equipped with a cold field emission gun and a spherical aberration corrector for probe correction.

3. Electrocatalytic testing

Electrocatalytic measurements were carried out in a commercial one-compartment three-electrode equipment at room temperature. The working electrodes were prepared by using the as-prepared catalysts, the samples of commercial 20 wt.% Pt/C and IrO₂, respectively. A platinized carbon electrode was utilized as the counter electrode, while a saturated calomel electrode (SCE) was used as the reference electrode that was attached to a commercial electrochemical workstation (CHI 760e, Shanghai, China). For the preparation of the working electrode, 5 mg of the as-prepared catalyst (commercial 20 wt.% Pt/C or IrO₂) was added into EtOH (1 mL) and 5% Nafion solution (50 μL), and then ultrasonicated for 30 min to prepare the ink. A 120 μL of the as-prepared ink was loaded onto one piece of 1 \times 3 cm² carbon paper (ca. 0.2 mg/cm²).

For all the measurements, the SCE reference electrode was pre-calibrated standardly with respect to reversible hydrogen electrode (RHE). Linear sweep voltammetry (LSV) measurement was conducted in electrolyte at a scan rate of 5 mV s⁻¹. All polarization curves were iR-corrected. The date of all the potentials reported in this study were obtained vs. RHE in 1 M KOH, by following the equation: $E(\text{RHE}) = E(\text{SCE}) + 1.052 \text{ V}$. The double-layer charging current is equal to the product of the scan rate, ν , and the electrochemical double-layer capacitance, C_{dl} , as given by Eq: $i_c = \nu C_{\text{dl}}$. Thus, a plot of i_c as a function of ν yields a straight line with a slope equal to C_{dl} . The TOF value was calculated from the formula: $\text{TOF} = I/4 nF$. Where 1/4 indicates that the formation of one oxygen molecule need four electrons, I represents the current (A) during the LSV measurement, F is the Faraday constant (96485 C mol⁻¹), and n is the number of active sites (mol).

4. Theoretical calculations

Model construction The model of bulk Co₂P was constructed with the space group of Pbnm, with the lattice parameters of $a = 6.638 \text{ \AA}$, $b = 5.670 \text{ \AA}$, $c = 3.52 \text{ \AA}$, and $\alpha = \beta = \gamma = 90^\circ$.¹ This bulk model of Co₂P was $2 \times 2 \times 2$ in the a -, b -, and c - directions. Thus the {001}, {010}, {100}, and {121} facets of bulk Co₂P were cleaved according to the optimized geometry of bulk Co₂P. Each facet model contains 4 layers of Co, 4 layers of P, and vacuum layer of 15 \AA . The models of Ni and Fe-doped Co₂P, named as (NiCo)₂P and (FeCo)₂P, respectively, were built in the similar way by substituting one fifth of the Co atoms with Ni or Fe atoms. By comparing the surface energies (Table S1), the {121} facets of Co₂P, (NiCo)₂P, and (FeCo)₂P were determined to be the preferably exposed facets.

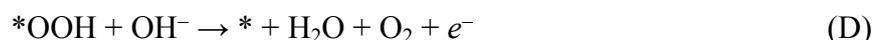
During OER test, the phosphides were oxidized to oxyhydroxides. Therefore, the model of CoOOH was constructed with the space group of P63/mmc. The lattice parameters were $a = b = 2.855 \text{ \AA}$, $c = 8.805 \text{ \AA}$, $\alpha = \beta = 90^\circ$, $\gamma = 120^\circ$.² The {001} facet of CoOOH was cleaved using the method mentioned above. The models of Ni and Fe-doped CoOOH, named as (NiCo)OOH and (FeCo)OOH, respectively, were built in the similar way by substituting one fifth of the Co atoms with Ni or Fe atoms.

Computational methods The quantum mechanic calculations were performed in the framework of density functional theory (DFT) using the DMol³ module of Materials Studio version 5.5 software package (Accelrys software inc., San Diego, CA).^{3,4} The exchange-correlation functional was chosen to be the Perdew-Burke-Ernzerhof (PBE) of generalized gradient approximation (GGA).⁵ In order to take the relativity effect into consideration, the density functional semicore pseudopotential (DSPP) method was applied for Co, Ni, and Fe elements, whereas the P, O, and H elements were dealt with an all-electron basis set. The valence electron functions were expanded into a set of numerical atomic orbitals with a double numerical basis with polarization functions (DNP). The geometry optimization was based on the following point: (1) an energy tolerance of 1.0×10^{-5} Hartree, (2) a displacement tolerance of $5.0 \times 10^{-3} \text{ \AA}$, (3) a force tolerance of 2.0×10^{-3} Hartree/ \AA . The surface energy (γ) was calculated with eq 1^{6,7}

$$\gamma = \frac{E_{\text{facet}} - E_{\text{bulk}}}{2A} \quad (1)$$

where E_{facet} was the total energy of the optimized facet model containing the same number of formula unit as the bulk model, E_{bulk} was the total energy of the bulk model, and A was the surface area of one side for the facet.

For OER, the Gibbs free energy change (ΔG) of each elementary step was calculated with the similar method in our previous work.^{8,9} In summary, OER mechanism in alkaline media was as follows:



The computational standard hydrogen electrode (SHE) approximation is applied.¹⁰ Thus, the reaction Gibbs free energies were calculated as follows.⁸⁻¹⁰

$$\Delta G_{\text{A}} = G_{*\text{OH}} + 0.5G_{\text{H}_2} - G_* - G_{\text{H}_2\text{O}} - eU - kT \ln 10 \cdot \text{pH} \quad (2)$$

$$\Delta G_{\text{B}} = G_{*\text{O}} + 0.5G_{\text{H}_2} - G_{*\text{OH}} - eU - kT \ln 10 \cdot \text{pH} \quad (3)$$

$$\Delta G_{\text{C}} = G_{*\text{OOH}} + 0.5G_{\text{H}_2} - G_{*\text{O}} - G_{\text{H}_2\text{O}} - eU - kT \ln 10 \cdot \text{pH} \quad (4)$$

$$\Delta G_{\text{D}} = G_* + 0.5G_{\text{H}_2} - G_{*\text{OOH}} + G_{\text{O}_2} - eU - kT \ln 10 \cdot \text{pH} \quad (5)$$

The Gibbs free energies of the reactants and products were obtained by calculating their vibrational frequencies.¹¹

For HER, the mechanism was as follows:



Thus, the Gibbs free energy change for HER were calculated with Eqs. 6 and 7.¹²

$$\Delta G_{\text{E}} = G_{*\text{H}} - G_* - 0.5G_{\text{H}_2} \quad (6)$$

$$\Delta G_{\text{F}} = G_* + 0.5G_{\text{H}_2} - G_{*\text{H}} \quad (7)$$

References

1. R. W. G. Wyckoff, Structures, *Cryst.*, 1963, **1**, 298.
2. M. Deliens, H. Goethals, *Mineral. Mag.*, 1973, **39**, 152.
3. B. Delley, *J. Chem. Phys.*, 1990, **92**, 508.
4. B. Delley, *J. Phys. Chem.*, 1996, **100**, 6107.
5. J. P. Perdew, K. Burke and M. Ernzerhof, *Phys. Rev. Lett.*, 1996, **77**, 3865.
6. D. Santos-Carballal, A. Roldan, R. Grau-Crespo and N. H. de Leeuw, *Phys. Chem. Chem. Phys.*, 2014, **16**, 21082.
7. F.-G. Wang, C. D. Valentin and G. Pacchioni, *J. Phys. Chem. C*, 2012, **116**, 10672.
8. S.-M. Xu, T. Pan, Y.-B. Dou, H. Yan, S.-T. Zhang, F.-Y. Ning, W.-Y. Shi and M. Wei, *J. Phys. Chem. C*, 2015, **119**, 18823.
9. S.-M. Xu, H. Yan and M. Wei, *J. Phys. Chem. C*, 2017, **121**, 2683.
10. A. Valdes, Z. W. Qu, G.-J. Kroes, J. Rossmeisl and J. K. Nørskov, *J. Phys. Chem. C*, 2008, **112**, 9872.
11. E. B. Wilson, J. C. Decius and P. C. Cross, *Molecular vibrations*; Dover: New York, 1980.
12. Y. Abghoui, E. Skulason, *J. Phys. Chem. C*, 2017, **121**, 24036.

Figure S1

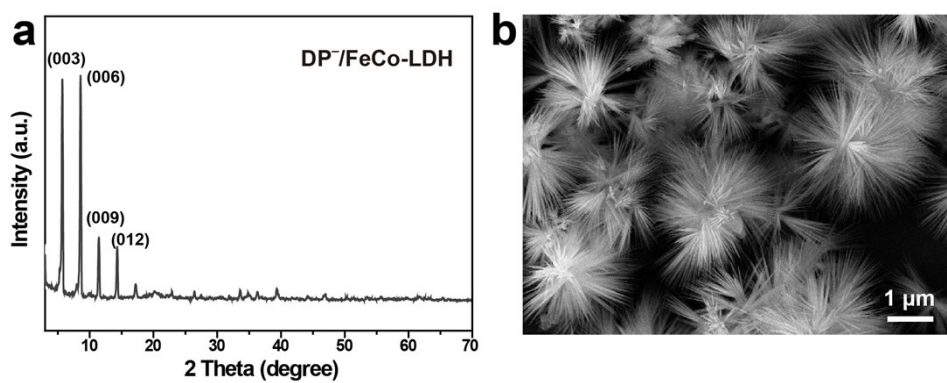


Fig. S1 (a) XRD pattern and (b) SEM image of the precursor of intercalated DP-/FeCo-LDH.

Figure S2

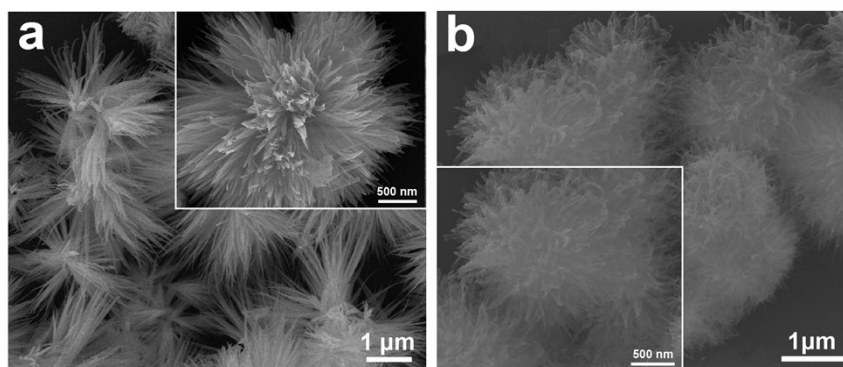


Fig. S2 SEM images of the echinus-like microspheres: (a) $(\text{Fe}_{0.2}\text{Co}_{0.8})_2\text{P}@C$ derived from a FeCo-LDH/ SDP^- precursor, and (b) $(\text{Ni}_{0.2}\text{Co}_{0.8})_2\text{P}@C$ microspheres derived from a NiCo-LDH/ SDP^- precursor.

Figure S3

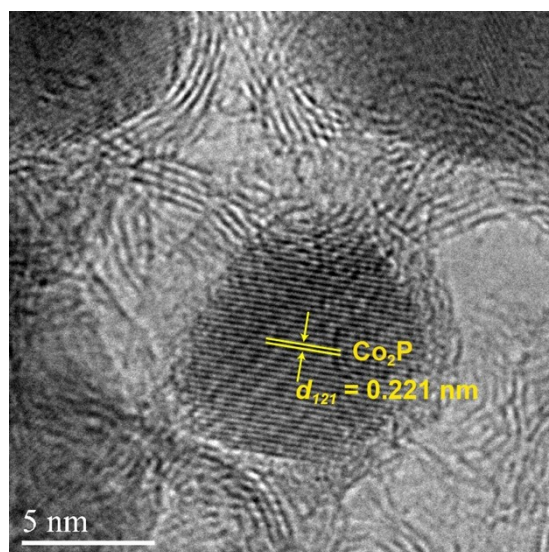


Fig. S3 HRTEM images of Co₂P@C microsphere derived from a Co(OH)₂/SDP⁻ host/guest precursor.

Figure S4

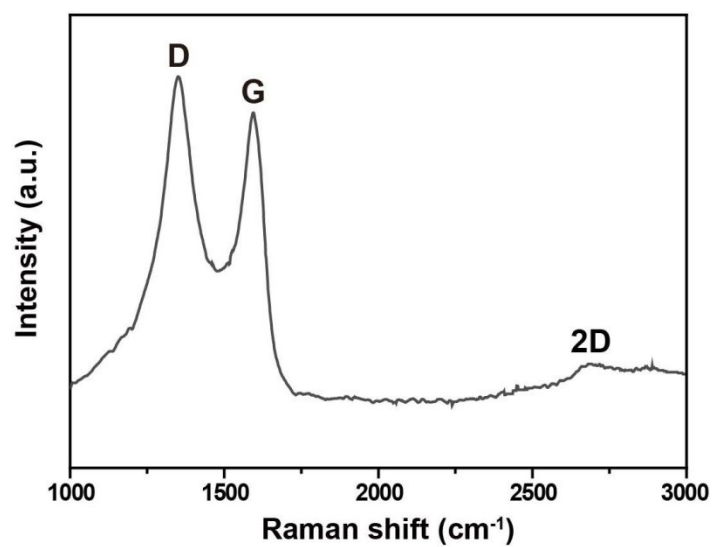


Fig. S4 Raman spectrum of the echinus-like $(\text{Fe}_{0.2}\text{Co}_{0.8})_2\text{P}@C$ composite.

Figure S5

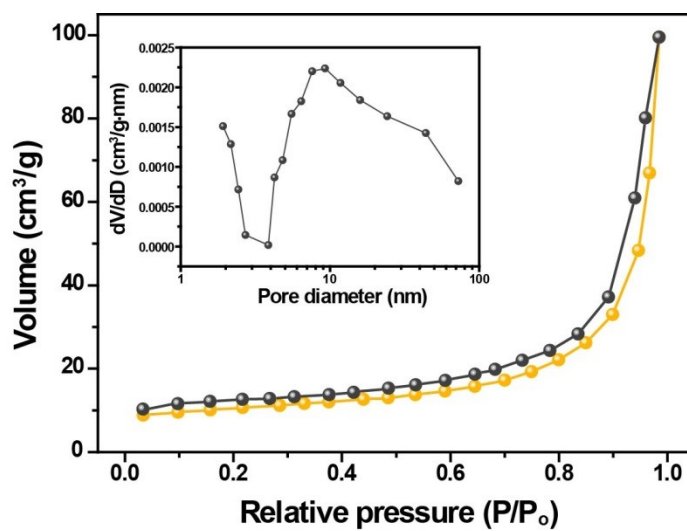


Fig. S5 Nitrogen adsorption/desorption isotherms, and pore size distribution of the $(\text{Fe}_{0.2}\text{Co}_{0.8})_2\text{P}@C$ composite.

Figure S6

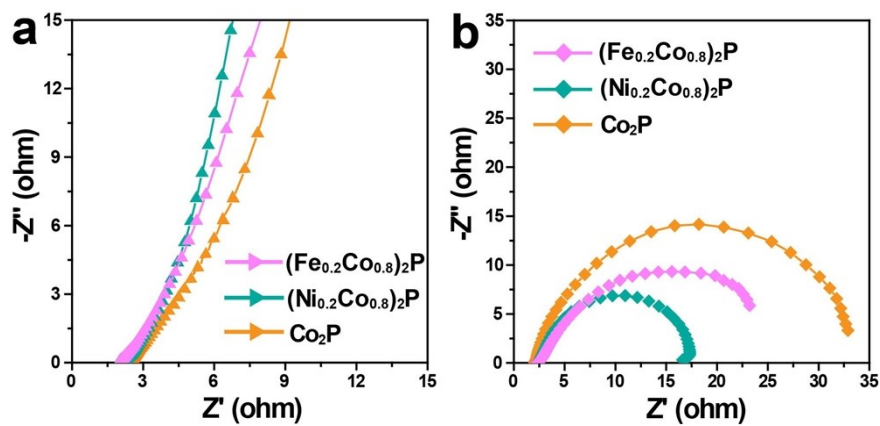


Fig. S6 Electrochemical impedance spectra of $(\text{Fe}_{0.2}\text{Co}_{0.8})_2\text{P}@C$, $(\text{Ni}_{0.2}\text{Co}_{0.8})_2\text{P}@C$ and $\text{Co}_2\text{P}@C$ composites for the (a) OER and (b) HER, respectively.

Figure S7

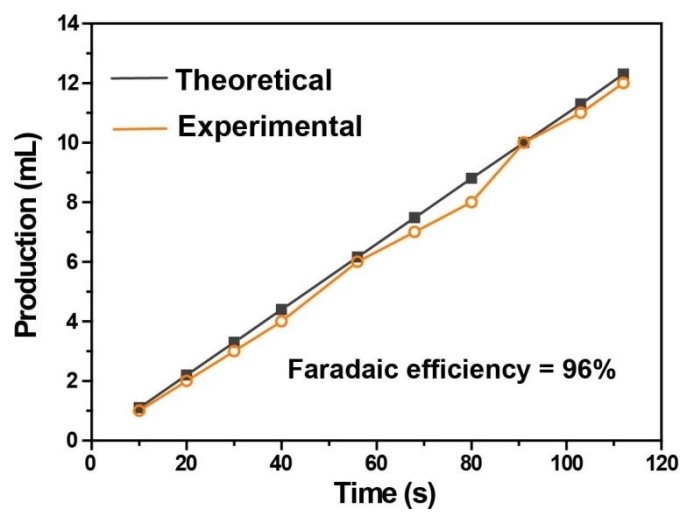


Fig. S7 Calculated and actual oxygen production catalyzed by $(\text{Fe}_{0.2}\text{Co}_{0.8})_2\text{P}@C$ at a constant current of 100 mA cm^{-2} .

Figure S8

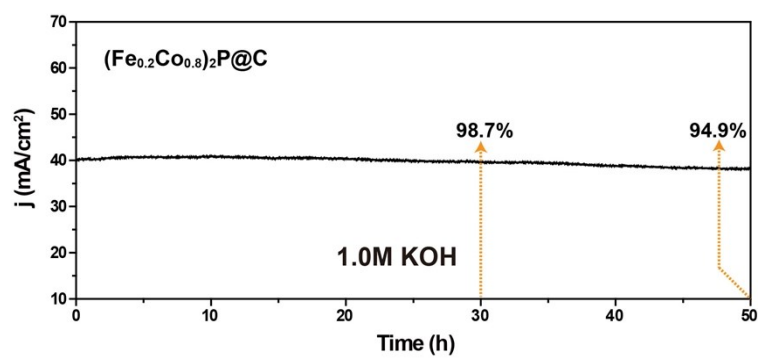


Fig. S8 Chronoamperometric curves of $(\text{Fe}_{0.2}\text{Co}_{0.8})_2\text{P}@C$ at an overpotential of 330 mV.

Figure S9

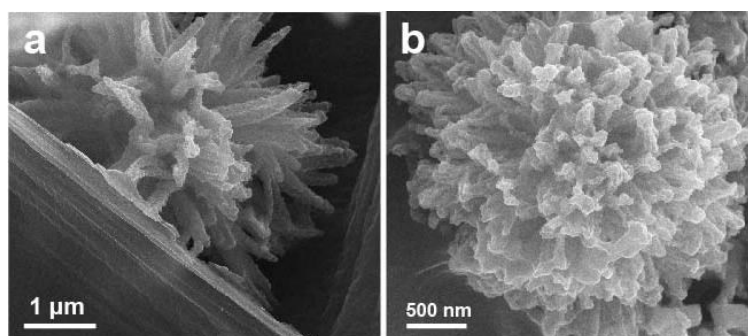


Fig. S9 (a) and (b) SEM images of the post-tested $(\text{Fe}_{0.2}\text{Co}_{0.8})_2\text{P}@C$ electrode which was prepared on carbon paper after 50 h of electrocatalytic testing.

Figure S10

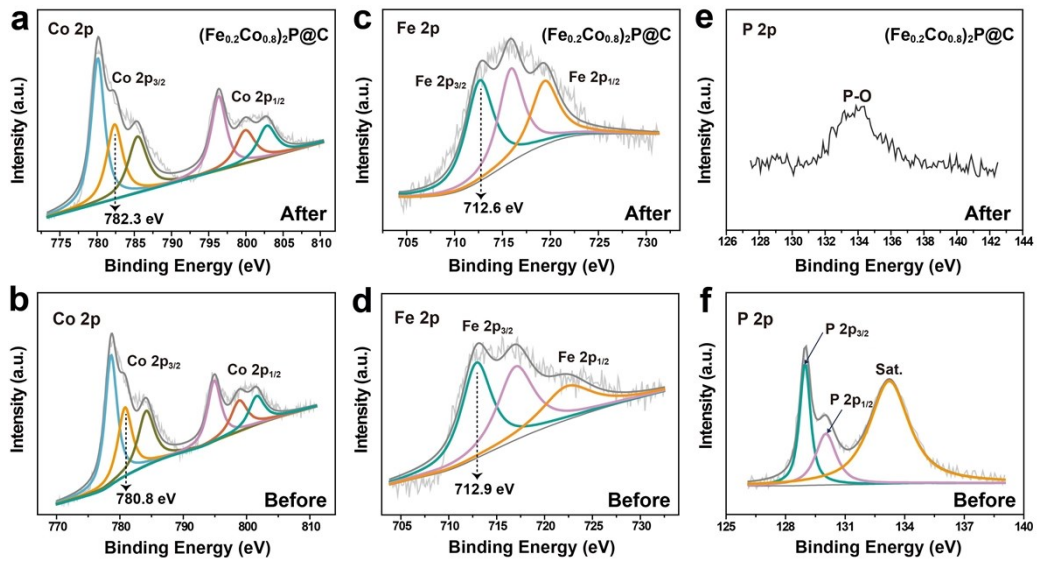


Fig. S10 Comparison of XPS spectra: (a,b) Co 2p, (c,d) Fe 2p, and (e,f) P 2p for the $(\text{Fe}_{0.2}\text{Co}_{0.8})_2\text{P@C}$ electrodes (a,c,e) after and (b,d, f) before the OER test.

Figure S11

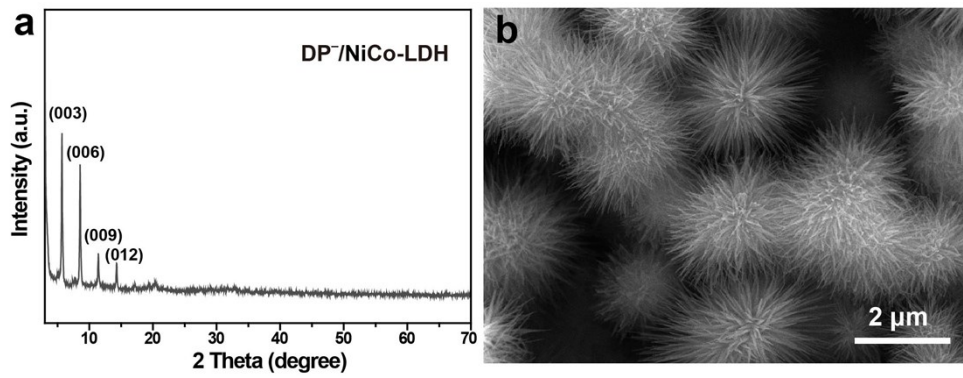


Fig. S11 (a) XRD pattern and (b) SEM image of a different precursor of SDP-intercalated NiCo-LDH.

Figure S12

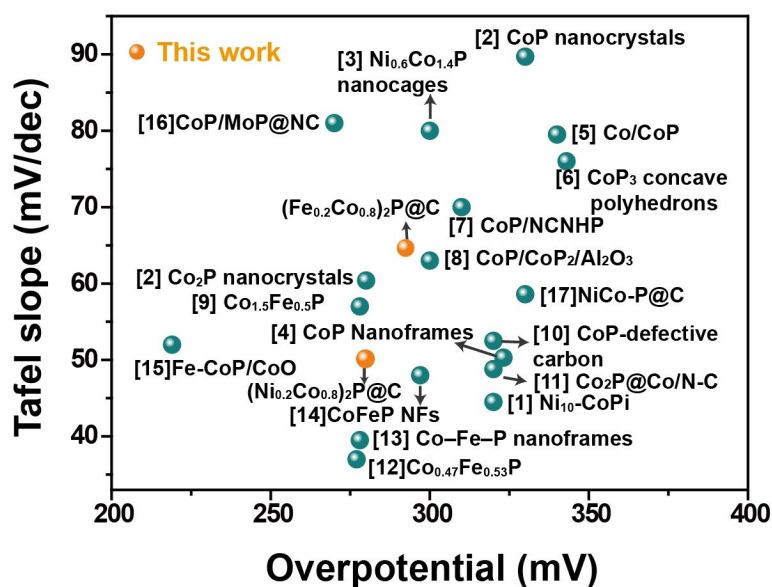


Fig. S12 Comparison of OER performance in alkaline electrolytes for $(\text{Fe}_{0.2}\text{Co}_{0.8})_2\text{P}@C$, $(\text{Ni}_{0.2}\text{Co}_{0.8})_2\text{P}@C$, and those Co-based TMP electrocatalysts reported previously.

Figure S13

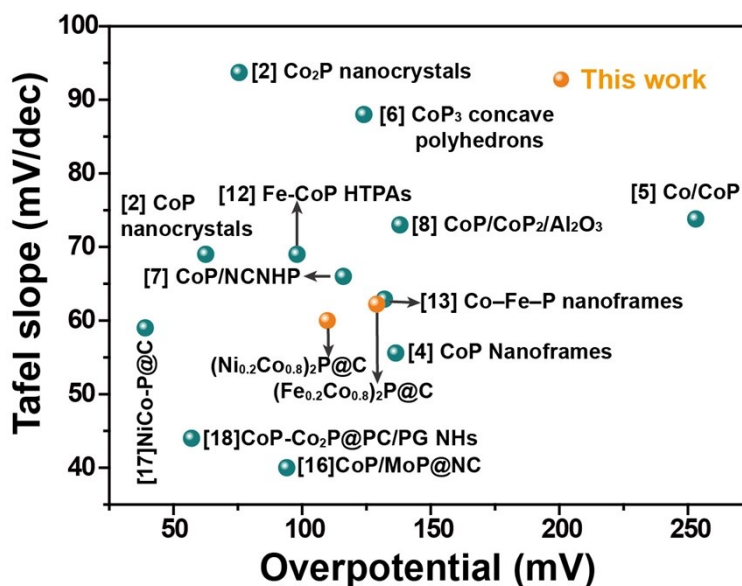


Fig. S13 Comparison of HER performance in alkaline electrolytes for $(\text{Fe}_{0.2}\text{Co}_{0.8})_2\text{P}@C$, $(\text{Ni}_{0.2}\text{Co}_{0.8})_2\text{P}@C$, and those Co-based TMP electrocatalysts reported previously.

References (for Figs. S12 and S13):

1. L. Yang, H. Ren, Q. Liang, K. N. Dinh, R. Dangol and Q. Yan, *Small*, 2020, **16**, 1906766.
2. H. Li, Q. Li, P. Wen, T. B. Williams, S. Adhikari, C. Dun, C. Lu, D. Itanze, L. Jiang,

- D. L. Carroll, G. L. Donati, P. M. Lundin, Y. Qiu and S. M. Geyer, *Adv. Mater.*, 2018, **30**, 1705796.
3. B. Qiu, L. Cai, Y. Wang, Z. Lin, Y. Zuo, M. Wang and Y. Chai, *Adv. Funct. Mater.*, 2018, **28**, 1706008.
 4. L. Ji, J. Wang, X. Teng, T. J. Meyer and Z. Chen, *ACS Catal.*, 2020, **10**, 412.
 5. Z.-H. Xue, H. Su, Q.-Y. Yu, B. Zhang, H.-H. Wang, X.-H. Li and J.-S. Chen, *Adv. Energy Mater.*, 2017, **7**, 1602355.
 6. T. Wu, M. Pi, X. Wang, D. Zhang and S. Chen, *Phys. Chem. Chem. Phys.*, 2017, **19**, 2104.
 7. Y. Pan, K. Sun, S. Liu, X. Cao, K. Wu, W.-C. Cheong, Z. Chen, Y. Wang, Y. Li, Y. Liu, D. Wang, Q. Peng, C. Chen and Y. Li, *J. Am. Chem. Soc.*, 2018, **140**, 2610.
 8. W. Li, S. Zhang, Q. Fan, F. Zhang and S. Xu, *Nanoscale*, 2017, **9**, 5677.
 9. S. Yang, G. Chen, A. G. Ricciardulli, P. Zhang, Z. Zhang, H. Shi, J. Ma, J. Zhang, P.W. M. Blom and X. Feng, *Angew. Chem. Int. Ed.*, 2020, **59**, 465.
 10. Y. Lin, L. Yang, Y. Zhang, H. Jiang, Z. Xiao, C. Wu, G. Zhang, J. Jiang and L. Song, *Adv. Energy Mater.*, 2018, **8**, 1703623.
 11. C. Zhu, S. Fu, B. Z. Xu, J. Song, Q. Shi, M. H. Engelhard, X. Li, S. P. Beckman, J. Sun, D. Du and Y. Lin, *Small*, 2017, **13**, 1700796.
 12. S. Yue, S. Wang, Q. Jiao, X. Feng, K. Zhan, Y. Dai, C. Feng, H. Li, T. Feng and Y. Zhao, *ChemSusChem*, 2019, **12**, 4461.
 13. W. Li, Y. Chen, B. Yu, Y. Hu, X. Wang and D. Yang, *Nanoscale*, 2019, **11**, 17031.
 14. Y. Lian, H. Sun, X. Wang, P. Qi, Q. Mu, Y. Chen, J. Ye, X. Zhao, Z. Deng and Y. Peng, *Chem. Sci.*, 2019, **10**, 464.
 15. X. Hu, S. Zhang, J. Sun, L. Yu, X. Qian, R. Hu, Y. Wang, H. Zhao and J. Zhu, *Nano Energy*, 2019, **56**, 109.
 16. Y.-J. Tang, H.-J. Zhu, L.-Z. Dong, A. Zhang, S.-L. Li, J. Liu and Y.-Q. Lan, *Appl. Catal. B: Environ.*, 2019, **245**, 528.
 17. V. H. Hoa, D. T. Tran, H. T. Le, N. H. Kim and J. H. Lee, *Appl. Catal. B*, 2019, **253**, 235.
 18. J. Yang, D. Guo, S. Zhao, Y. Lin, R. Yang, D. Xu, N. Shi, X. Zhang, L. Lu, Y.-Q. Lan, J. Bao and M. Han, *Small*, 2019, **15**, 1804546.

Figure S14

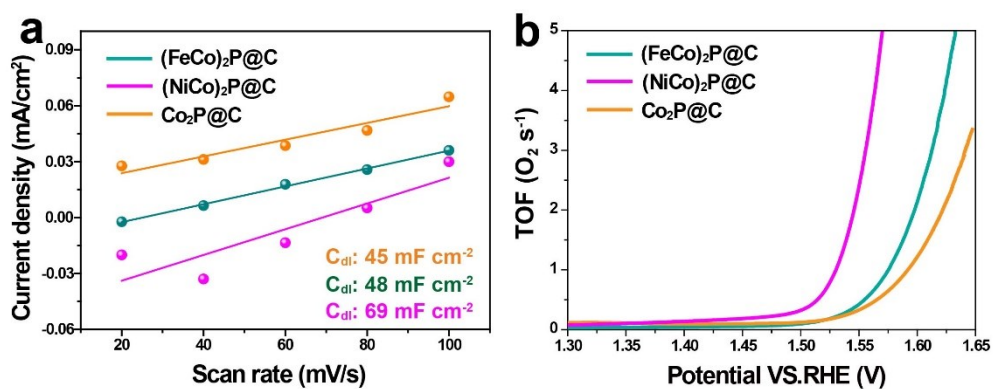


Fig. S14 (a) The capacitive currents (at 0.15 V vs SCE) as a function of scan rates (from 20 to 100 mV s⁻¹) for (Fe_{0.2}Co_{0.8})₂P@C, (Ni_{0.2}Co_{0.8})₂P@C, and Co₂P@C. (b) Calculated TOF of (Fe_{0.2}Co_{0.8})₂P@C, (Ni_{0.2}Co_{0.8})₂P@C, and Co₂P@C.

Figure S15

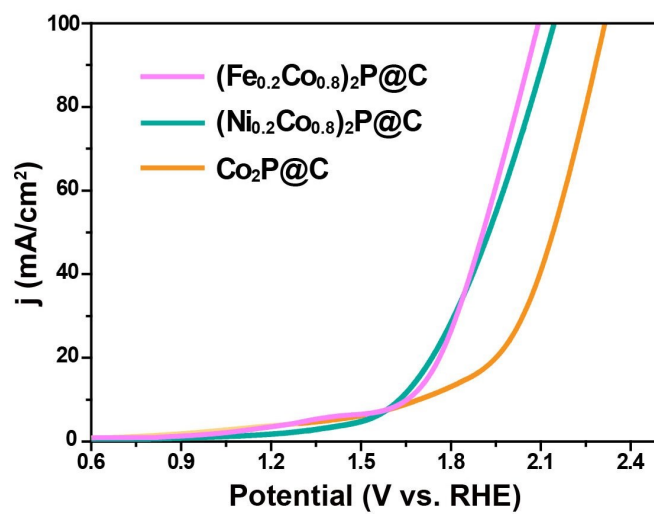


Fig. S15 Polarization curves of the assembled $(\text{MCo})_2\text{P}@C||(\text{MCo})_2\text{P}@C$ systems for overall water splitting in 1.0 M KOH: $\text{Co}_2\text{P}@C||\text{Co}_2\text{P}@C$, $(\text{Fe}_{0.2}\text{Co}_{0.8})_2\text{P}@C||(\text{Fe}_{0.2}\text{Co}_{0.8})_2\text{P}@C$, and $(\text{Ni}_{0.2}\text{Co}_{0.8})_2\text{P}@C||(\text{Ni}_{0.2}\text{Co}_{0.8})_2\text{P}@C$.

Figure 16

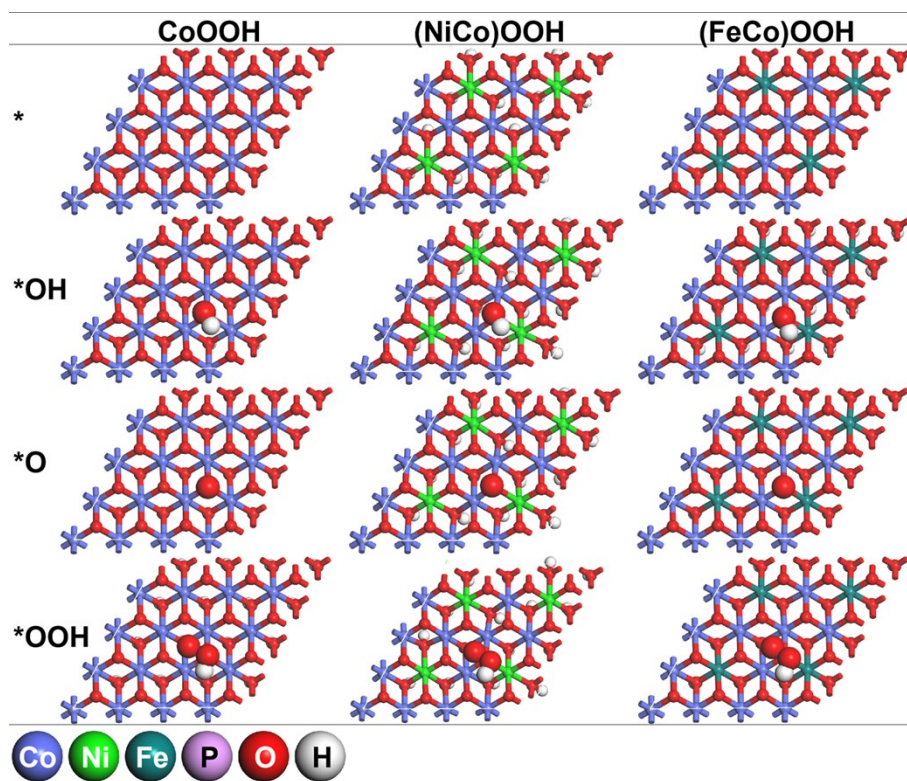


Fig. S16 Optimized geometries of OER intermediates for CoOOH, (Ni_{0.2}Co_{0.8})OOH, and (Fe_{0.2}Co_{0.8})OOH. The color of each element is labeled.

Figure S17

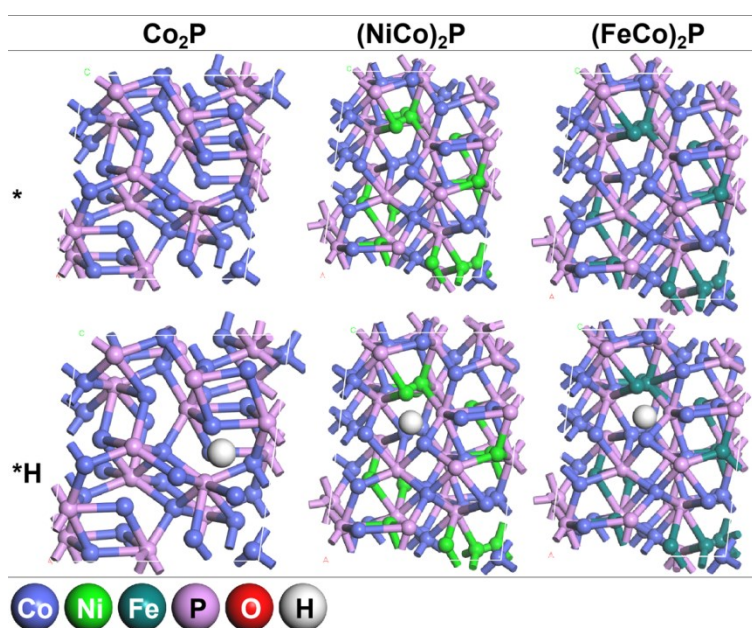


Fig. S17 Optimized geometries of HER intermediates for Co_2P , $(\text{Ni}_{0.2}\text{Co}_{0.8})_2\text{P}$, and $(\text{Fe}_{0.2}\text{Co}_{0.8})_2\text{P}@C$. The color of each element is labeled.

To further confirm the preferably exposed facet of Co_2P , $(\text{Ni}_{0.2}\text{Co}_{0.8})_2\text{P}$, and $(\text{Fe}_{0.2}\text{Co}_{0.8})_2\text{P}$, the surface energies of (121), and three low-index facets, (001), (010), and (100), are calculated with *eq 1*. The detailed energies of the bulk model and facet models for each phosphide are listed in Table S1. As shown, the surface energy of the (121) facet is lower than those of the other three facets, unraveling that the (121) facet is more stable than the other calculated facets. The surface energies of (121) facets are the smallest for $(\text{Fe}_{0.2}\text{Co}_{0.8})_2\text{P}$, $(\text{Ni}_{0.2}\text{Co}_{0.8})_2\text{P}$, and Co_2P . Therefore, the (121) facets are determined to be the preferably exposed facet and employed in the further reaction mechanism calculations.

Figure S18

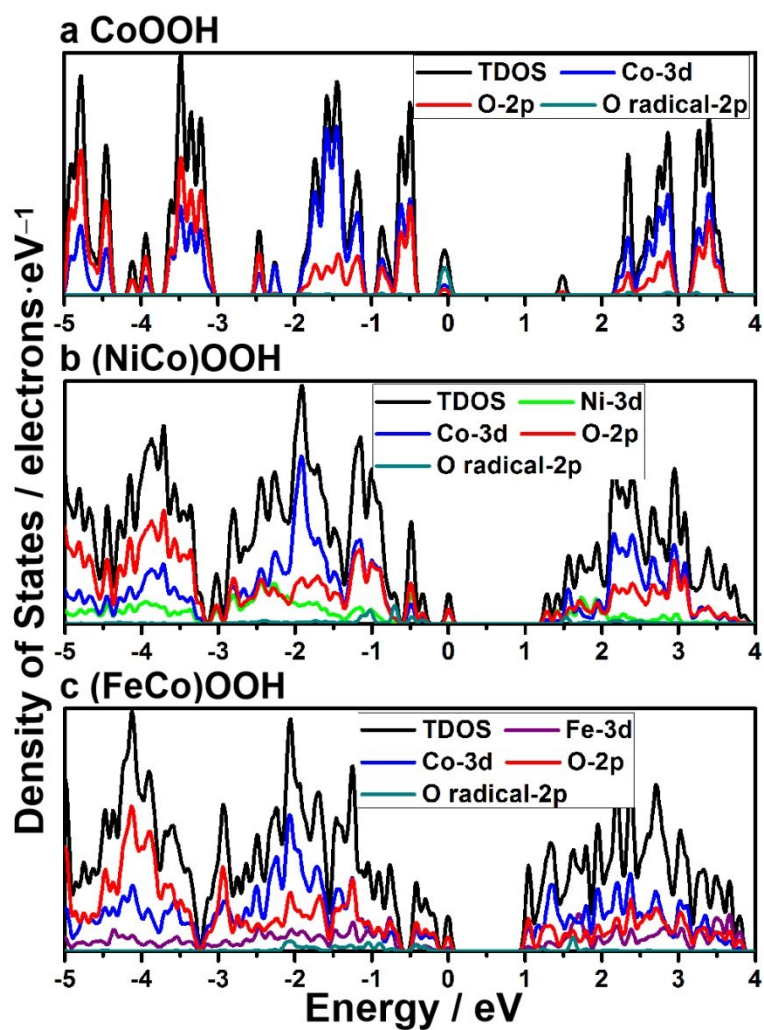


Fig. S18 Total and partial density of states for CoOOH, (NiCo)OOH, and (FeCo)OOH.

Table S1

Energy, surface area, and surface energy (γ) of each calculated facet for Co_2P , $(\text{NiCo})_2\text{P}$, and $(\text{FeCo})_2\text{P}$.

sample	model	energy / eV	$A / \text{\AA}^2$	$\gamma / \text{J}\cdot\text{m}^{-2}$
Co_2P	bulk	-18095.4355		
	(001)	-18093.5969	19.84	0.7413
	(010)	-18089.5476	37.32	1.2620
	(100)	-18092.8886	23.21	0.8779
	(121)	-18094.7021	80.65	0.0727
$(\text{FeCo})_2\text{P}$	bulk	-34780.3365		
	(001)	-34775.6451	39.68	0.9457
	(010)	-34775.9078	37.33	0.9492
	(100)	-34775.5208	46.41	0.8300
	(121)	-34776.1559	96.44	0.3468
$(\text{NiCo})_2\text{P}$	bulk	-38712.0395		
	(001)	-38705.8487	39.69	1.2480
	(010)	-38704.7992	37.32	1.5519
	(100)	-38703.0925	46.42	1.5420
	(121)	-38707.8171	96.45	0.3502